crystals

MDPI

Article

Preparation of Hierarchical Co/Beta Catalyst and Its Application in Hydrogenation of CO to Aviation Kerosene

Yanliang Zhai [1], Wanli Zhang [1], Xianggang Lu [1], Jun Wang [1], Jian Zhang [1], Lili Ma [2], Zhixiang Zhang [2] and Zhijun Li [1,*]

[1] Provincial Key Laboratory of Polyolefin New Materials, College of Chemistry & Chemical Engineering, Northeast Petroleum University, Daqing 163318, China; zhaiyl2010@163.com (Y.Z.)
[2] Daqing Chemical Research Center, Petrochemical Research Institute, Daqing 163714, China
* Correspondence: zhijun.li@queensu.ca

Abstract: Due to the increasing depletion of petroleum resources, the production route of non-oil-based aviation kerosene has been paid more and more attention. In this regard, the process of preparing aviation kerosene from syngas (CO and H_2) is one of the most promising industrial alternative fuel production routes. The traditional syngas-to-aviation kerosene catalyst uses iron-based and cobalt-based catalysts, which is a complex process with a high cost. In this work, a hierarchical Co/Beta metal-zeolite bifunctional catalyst prepared via the melting method is reported, which can directly and highly selectively produce an aviation kerosene component from syngas (CO and H_2). Compared with the catalyst prepared via the impregnation method, the Co/Beta catalyst prepared via the melting method has smaller, more highly dispersed Co metal active species and more suitable acid properties, the conversion of CO can reach 34.6%, and the selectivity of the C_8-C_{16} aviation kerosene component can reach 40.2%, which provides a new idea for the industrial production of aviation kerosene.

Keywords: Fischer–Tropsch synthesis; aviation kerosene; metal-zeolite bifunctional catalyst; hierarchical pore; acid property

check for updates

Citation: Zhai, Y.; Zhang, W.; Lu, X.; Wang, J.; Zhang, J.; Ma, L.; Zhang, Z.; Li, Z. Preparation of Hierarchical Co/Beta Catalyst and Its Application in Hydrogenation of CO to Aviation Kerosene. *Crystals* **2023**, *13*, 1053. https://doi.org/10.3390/cryst13071053

Academic Editors: Younes Hanifehpour and Yael Diskin-Posner

Received: 9 May 2023
Revised: 22 June 2023
Accepted: 28 June 2023
Published: 3 July 2023

Copyright: © 2023 by the authors. Licensee MDPI, Basel, Switzerland. This article is an open access article distributed under the terms and conditions of the Creative Commons Attribution (CC BY) license (https://creativecommons.org/licenses/by/4.0/).

1. Introduction

Aviation kerosene, also known as jet fuel, is mainly used as jet engine fuel. The main components of aviation kerosene are C_8-C_{16} normal isomeric alkanes and cycloalkanes, as well as a small amount of aromatics and olefins.

In recent years, the world air transport industry has developed rapidly. As far as the civil aviation industry is concerned, the average annual growth rate of personnel air transportation and material transportation is 4.9% and 5.3%, respectively. The annual global consumption of aviation fuel was approximately 300 Mt in 2017. It has been projected to rise to more than double that figure by 2050 [1].

Due to the rapid growth in the demand for aviation kerosene, the production of aviation kerosene has attracted more and more attention. The traditional production mode of aviation kerosene is crude oil distillation, and then the distilled kerosene fraction is hydrotreated and hydrocracked to produce aviation kerosene which meets the international standard.

A typical aviation kerosene component derives from petroleum. However, this process is heavily dependent on oil resources and requires highly specific equipment and materials. As we all know, global oil resources are becoming increasingly exhausted, so the development of alternative technologies for the preparation of aviation kerosene has attracted wide attention all over the world.

As a bridge of energy conversion, syngas, derived from coal, natural gas and biomass, can be converted into clean aviation kerosene. The route of preparing aviation kerosene from syngas (CO and H_2) is considered to be an alternative method of aviation kerosene

production with the greatest potential for large-scale industrialization. In this route, syngas is prepared from non-oil resources such as coal and natural gas, and then it is converted to liquid fuel via catalytic conversion of syngas. The physical–chemical properties of Fischer–Tropsch synthetic fuel are similar to those of traditional aviation fuel. Moreover, it contains less sulfur and nitrogen, which can reduce aero-engine pollution emissions [2,3].

The traditional syngas-to-aviation kerosene catalyst uses iron-based and cobalt-based catalysts, a process with high complexity and high cost. In 2008, the process of preparing aviation kerosene from syngas, developed by Sasol Company [4,5], first converted syngas to hydrocarbons via Fischer–Tropsch synthesis, and then the final products were obtained by hydrocracking, oligomerization, hydrofining, aromatization, alkylation and other processes. This process is a typical traditional process of producing aviation kerosene from syngas, which is complex and high in cost.

The new metal-zeolite bifunctional catalyst can realize the direct and highly selective preparation of aviation kerosene from syngas (CO and H_2) in one step. This new catalytic process route greatly simplifies the process flow and greatly reduces the process cost. It provides an important new idea for the industrial production of aviation kerosene and is expected to become an important alternative route for the production of aviation kerosene in the future.

Guan et al. [6] introduced "Al species" (the active center of acid catalysis) into the support of SBA-15 mesoporous zeolite by "pH regulation method", and they successfully synthesized a Co/Al-SBA-15 bifunctional catalyst. The Co-based catalyst with an Al/Si ratio of 0.01 exhibited the highest CO conversion (36.8%) and selectivity (52.4%) for aviation fuel (C_8-C_{18} products). The method is simple to operate and can be used to directly and selectively prepare aviation kerosene from syngas. However, the high cost of the SBA-15 zeolite and Ru metal limits the industrial application of the above catalysts.

Beta zeolite has a three-dimensional 12-membered ring channel structure, which provides a more regular space for metal loading. This promotes the dispersion of metal active sites on Beta zeolite support in the form of nanoparticles or subnanoparticles. Bifunctional Co-Beta catalysts with suitable metal active sites and acid sites have been prepared, making it possible to improve the selectivity of the C_8-C_{16} aviation kerosene component from syngas (CO and H_2)-to-aviation kerosene. More importantly, the cost of Co-Beta catalysts is low, and their industrial application is expected to be realized. Boymans et al. [7] prepared three types of zeolite supports (mesoZSM-5, mesoBeta and mesoY) by alkali treatment method, and then they used these supports to prepare three types of catalysts (Co/H-mesoZSM-5, Co/H-mesoBeta and Co/H-mesoY) via the impregnation method. Under the following reaction conditions, T = 240 °C, P = 20 bar and H_2/CO = 2, the Co/H-mesoBeta catalyst shows the highest selectivity of C_8-C_{16} (41.0%) aviation kerosene components and a relatively high CO conversion (32.8%).

Some research groups have also studied the effects of different temperatures, pressure and H_2/CO ratios on the catalytic performance of Co-based catalysts for converting syngas to aviation kerosene. It was found that higher reaction temperature was beneficial to the improvement of selectivity of low-carbon hydrocarbons such as C_2-C_{10}. This is due to the increase in temperature promoting the hydrocracking activity of zeolites, resulting in higher selectivity of low-carbon hydrocarbons in the products [7,8]. With the increase in the H_2/CO ratio in the syngas, the CO conversion is enhanced, the ratio of olefin to paraffin (O/P) in the hydrocarbon products is decreased slightly, and methane selectivity is increased, whereas the heavier hydrocarbons such as C_{5+} are reduced [9]. Increasing operating pressure, the CO conversion increases, the O/P ratio decreases slightly, the heavier hydrocarbons such as C_{5+} are enhanced [10].

In order to further improve the dispersion and catalytic activity of metal active centers, scholars are constantly developing new synthesis processes to control the morphology of catalysts, reduce the particle size of active components and improve the dispersion of metal centers [11]. In this work, a new preparation method of a hierarchical Co/Beta catalyst is proposed via a two-step method. The first step is to prepare a hierarchical Beta zeolite

support via acid treatment, the second step is to prepare a hierarchical Co/Beta catalyst via the melting method. Another series of Co-Beta catalysts with different cobalt loading were prepared via the impregnation method for comparison. The effects of cobalt loading and catalyst preparation methods on the active species differentiation, acid properties and Fischer–Tropsch catalytic performance of hierarchical Co-Beta catalysts were studied. This work provides theoretical guidance for the design and development of industrial catalysts for the direct and highly selective synthesis of aviation kerosene from syngas.

2. Materials and Methods

2.1. Materials

Nitric acid and Cobalt nitrate hexahydrate ($Co(NO_3)_2 \cdot 6H_2O$, AR) were purchased from Macklin Biochemical Co., Ltd. (Shanghai, China). The H-type Beta zeolite (SiO_2/Al_2O_3 = 25) was purchased from Catalyst Plant of Nankai University. All reactants were used as received, without further purification.

2.2. Catalysts Preparation

2.2.1. Beta Zeolite Pretreatment

Add 10 g H-type Beta zeolite (SiO_2/Al_2O_3 = 25) to the nitric acid solution (2 mol/L) of 150 mL and then treat it in a water bath at 90 °C under constant temperature reflux and stirring for 12 h. Then, after washing twice with deionized water, the obtained zeolites were dried overnight in an oven at 100 °C to obtain H-type Beta zeolites with hierarchical structure treated by acid. The original Beta zeolite is named BP, and the zeolite treated with nitric acid is named BN.

2.2.2. Preparation of Hierarchical Co/Beta Catalysts by Impregnation

The cobalt nitrate aqueous solution with a certain amount of cobalt loading (1 wt%, 3 wt%, 5 wt%, 10 wt% Co) was added to the acid-treated Beta zeolite powder drop by drop, and the cobalt nitrate aqueous solution was stirred continuously to make it fully mixed; then, it was stirred for 0.5 h and impregnated overnight at room temperature. Then, the sample was dried in an oven at 100 °C for 8 h and then calcined at 550 °C with a heating rate of 10 °C/min in the air for 6 h. The series of hierarchical Co/Beta catalysts prepared by impregnation are named xCB-IM, where x represents the loading amount of Co (x = 1, 3, 5 and 10).

2.2.3. Preparation of Hierarchical Co/Beta Catalysts via the melting method

The mixture of $Co(NO_3)_2 \cdot 6H_2O$ and Beta zeolite (cobalt loading 10 wt%) was physically mixed in a mortar for 0.5 h, and then it was transferred to a sealed glass bottle and heated in an oven at 80 °C for 8 h. At 80 °C, $Co(NO_3)_2 \cdot 6H_2O$ changes into molten state, and $Co(NO_3)_2 \cdot 6H_2O$ in molten state has certain fluidity and can penetrate into the micropores and mesoporous channels of hierarchical Beta zeolites. The hierarchical Co/Beta catalyst prepared via the melting method was obtained by calcining it in a muffle furnace at 550 °C for 6 h. The hierarchical Co/Beta catalysts prepared via the melting method are named 10CB-MM, in which 10 represents the loading amount of Co.

2.3. Characterization

The X-ray powder diffraction (XRD) patterns were obtained on a Rigaku D/MAX-2200 X-ray diffractometer (Rigaku Corporation, Tokyo, Japan) with Cu Kα radiation (λ = 1.5406 Å). High-resolution transmission electron microscopy (TEM) characterization was recorded on an FEI TECNAI G2 F20 (FEI, Hillsboro, OR, USA) at an acceleration voltage of 200 kV.

N_2 adsorption–desorption was performed on a Micromeritics ASAP 2460 (Micromeritics, Norcross, GA, USA). The total surface areas were calculated by the BET method. The internal/external surface area and micropore volume were determined by the t-plot method, while the mesopore volume was determined by the BJH method.

UV–Vis spectroscopy was performed on a Shimadzu UV-3600 (Shimadzu, Tokyo, Japan). Ammonia temperature programmed desorption (NH_3-TPD) was conducted using a Xianquan TP-5076 adsorption instrument with a thermal conductivity detector (TCD) (Xianquan, Tianjin, China).

H_2 temperature-programmed reduction (H_2-TPR) was conducted using a Xianquan TP-5080 adsorption instrument with a thermal conductivity detector (TCD) (Xianquan, Tianjin, China). A 0.1 g sample is purged and activated at 100 °C in N_2 atmosphere for 1 h. Then, a mixture of H_2 and N_2 (5 vol% H_2, 50 mL/min) is injected, and the temperature is raised from 100 °C to 800 °C at a rate of 10 °C/min, while the H_2 signal is analyzed and recorded by TCD.

2.4. Catalytic Reaction

Fischer–Tropsch synthesis was performed in a stainless-steel reactor (inner diameter = 8mm). A sample of 0.5 g mixed with 1.0 g quartz sand was pretreated in H_2 gas at a flow rate of 30 mL/min and 400 °C for 8 h. After the reactor was cooled to 230 °C, syngas with a H_2/CO ratio of 2 and a flow rate of 26 mL/min was introduced into the reactor, and the GHSV was 3120 mL/(g_{cat}·h). Then, the pressure was raised to 3 MPa to start the Fischer–Tropsch reaction. The gas products were monitored by online gas chromatography with Agilent 7890A chromatographs (TCD and FID). An ice trap was employed to capture the liquid hydrocarbons in the effluent. The liquid products with 0.1 g of an internal standard (n-C_{14}) were analyzed using an off-line Shimadzu GC-2014 (FID) (Shimadzu, Tokyo, Japan). The calculation of hydrocarbon selectivity was based on the mole fraction of a product with respect to the total hydrocarbons.

3. Results and Discussion

Figure 1 shows the XRD patterns of the Co/Beta catalysts. All these samples exhibit typical diffraction peaks of Beta zeolite at 2θ = 7.3° and 22.2° (marked with rhomboid, JCPDS 48-0074), indicating that the samples contain the Beta zeolite phase as the support of Co/Beta catalysts with high crystallinity [12,13]. Moreover, for the Co/Beta series catalysts prepared via the impregnation method, the diffraction peaks at 2θ = 7.3° and 22.2° decreased gradually with the increase in cobalt loading, which indicated that the characteristic diffraction peaks of Beta zeolites were weakened after loading cobalt. The catalyst is composed of cobalt oxide and Beta zeolite, and when the cobalt loading amount increases, the proportion of Beta zeolite crystal phase in the whole catalyst crystal decreases, so the characteristic diffraction peak intensity of Beta zeolite crystal phase decreases gradually. In addition, compared with the sample BN, it is found that the samples 5CB-IM, 10CB-IM and 10CB-MM show weaker characteristic diffraction peaks at 2θ = 31.7°, 36.9°, 59.4° and 65.4° (marked with heart), which were attributed to (220), (311), (511) and (440) reflections of Co_3O_4, and the diffraction peak of these angles increases with the increase in cobalt loading [14]. The above XRD characterization shows that we have successfully prepared Co/Beta catalysts via the impregnation method and melting method.

In order to characterize the crystal size and morphology of the catalysts, a series of Co-Beta catalysts were characterized by SEM, as shown in Figure 2. It can be seen from Figure 2 that the crystal size of the original Beta zeolite BP sample is about the same as the larger particles of 200 nm, the surface of the zeolite particles is relatively smooth, and the particle morphology shows a relatively regular approximate octahedral morphology. After treatment with a higher concentration of nitric acid, whether 1CB-IM and 10CB-IM prepared via the impregnation method or 10CB-MM prepared via the melting method, the catalyst samples show rough nanocrystalline-morphology, and the secondary particles of 200 nm each are formed by the primary particles of 20–30 nm. This is because during the dealumination and partial dissolution of Beta zeolite in the acid treatment, the morphology of catalysts are changed, the surface becomes rougher, some zeolites appears holes after etching, and some zeolites are dissolved into smaller grains and accumulate to form a nanocrystalline-aggregated morphology. And, the accumulation of 20–30 nm nanoparticles

produces a large number of intercrystalline mesopores [15,16]. Thus, the hierarchical Co/Beta zeolite catalyst with a nanocrystalline-aggregated structure was formed.

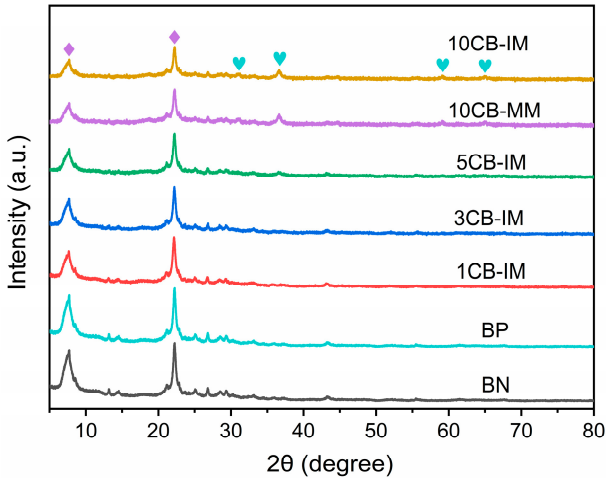


Figure 1. XRD patterns of different samples.

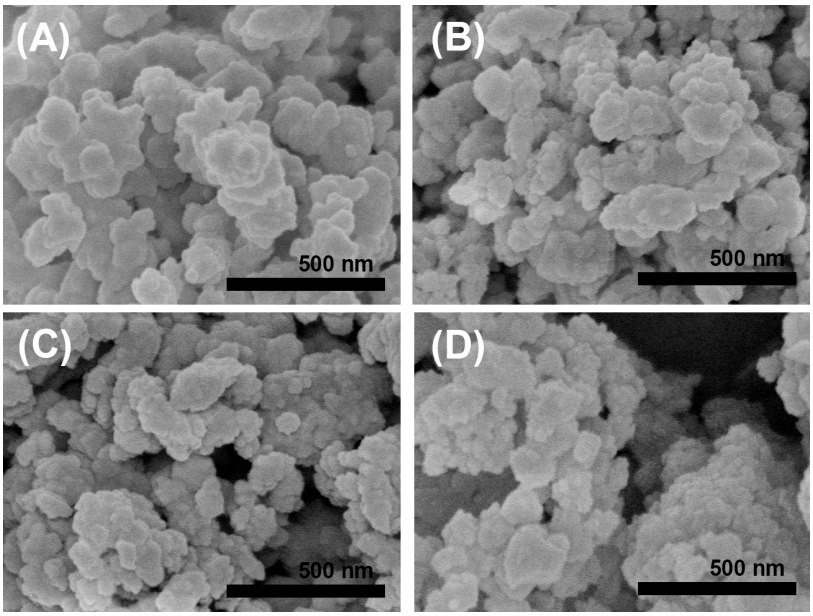


Figure 2. SEM images of BP (**A**), 1CB-IM (**B**), 10CB-MM (**C**), and 10CB-IM (**D**).

Figure 3 shows the TEM images of Co-Beta series of catalysts. It can be seen from Figure 3 that the crystal size of the original Beta zeolite BP sample is about 200 nm, and the surface of the zeolite particles is relatively smooth, and the particle morphology shows approximate octahedral morphology. After acid treatment and Co impregnation, 1CB-IM and 10CB-IM prepared via the impregnation method show rough nanocrystalline-aggregated morphology, and the secondary particle of 200 nm is formed by the primary particles of 20–50 nm. Meanwhile, with acid treatment and cobalt melting, 10CB-MM prepared via the melting method show a rough nanocrystalline-aggregated morphology with a loose and porous morphology, and the secondary particle of 150 nm is formed by the primary particles of 20–30 nm. This is caused by a high concentration of nitric acid treatment. During the acid treatment, the framework aluminums of Beta zeolite are partially removed, and the Beta zeolite particles are partially dissolved and become smaller. This process forms large numbers of intercrystalline mesopores and obtains a hierarchical Co/Beta catalyst with nanocrystalline-aggregated morphology [15,17]. By observing the TEM images of the 10CB-MM and 10CB-IM catalyst samples with high magnification

(Figure S1), it is found that the cobalt species particles of the 10CB-MM samples prepared via the melting method are smaller and more uniformly dispersed, with a particle size of about 5–10 nm, while that of the 10CB-IM samples prepared via the impregnation method is larger, with a particle size of about 8–20 nm.

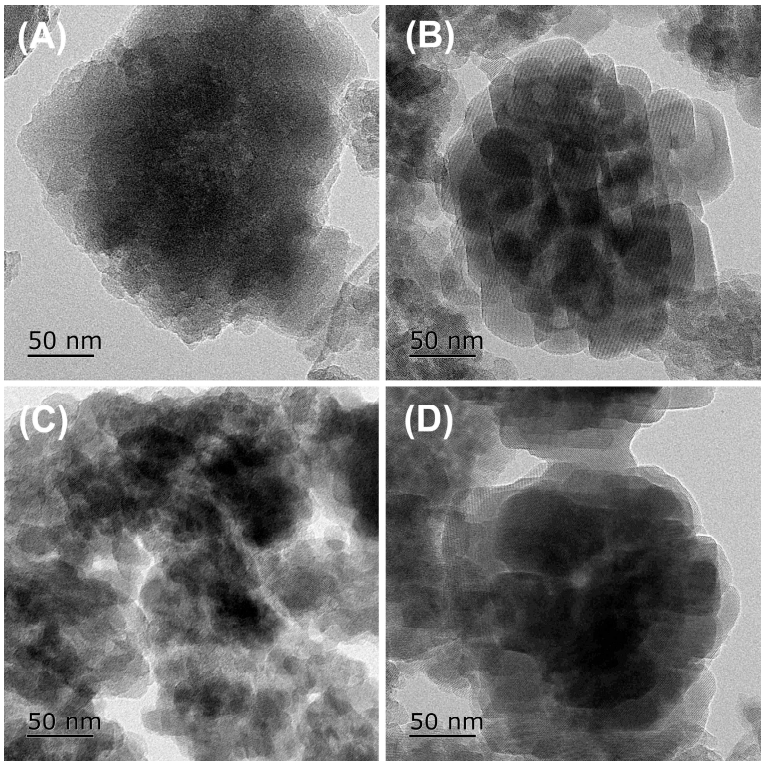


Figure 3. TEM images of BP (**A**), 1CB-IM (**B**), 10CB-MM (**C**), and 10CB-IM (**D**).

The pore structure properties of Co/Beta series catalysts were determined by N_2 adsorption–desorption method. The N_2 adsorption–desorption isotherms of different samples are shown in Figure 4. The total surface areas of different samples were calculated by the Brunauer–Emmett–Teller (BET) method. The internal/external surface area and micropore volume were determined by the t-plot method, while the mesopore volume was determined by the BJH method. As shown in Figure 4 and Table 1, compared with the sample BP before acid treatment and the sample BN after acid treatment, it was found that the surface area and pore volume of Beta zeolite increased after acid treatment; in particular, the mesopore volume increased obviously. Combined with the TEM characterization results, we can know this is due to the dealumination and partial dissolution of Beta zeolites treated with nitric acid, resulting in the accumulation of nanocrystals and the formation of a large number of intercrystalline mesopores. At the same time, all samples have a H3 hysteresis ring, which indicates that the mesoporous pore size distribution of catalyst samples is uneven and the pore size distribution range is wide. This is due to the uncontrollable mesoporous morphology, size and distribution produced by acid treatment, which can also be reflected in the pore size distribution curves below. This can be further confirmed by the characterization results of TEM (Figure 3 and Figure S1).

The textural properties of these samples are listed in Table 1. Compared with the BP sample without acid treatment, the total surface area, total pore volume and mesopore volume of acid-treated BN samples are significantly increased. Such high specific surface area (515 m^2/g) and mesoporous volume (0.44 cm^3/g) of BN sample are attributed to the well-developed intercrystalline mesoporous channels provided by a nanocrystalline-aggregated structure formed by acid treatment. As a catalyst support, this zeolite greatly improves the diffusion and mass transfer performance of the catalyst, and is beneficial

to improve the catalytic performance of syngas (CO and H_2) to aviation kerosene. With increasing Co loading amount, the external surface area and mesopore volume of the xCB-IM samples present a slightly decreasing trend. This is because the impregnated cobalt ions exchange with protons in the zeolite and generate CoO_x species after calcination, and are small and easily mobile. The small CoO_x species can migrate to the intercrystalline mesopore and external surface, gather and grow, resulting in a decrease in the external surface area and mesopore volume, while for the 10CB-MM samples prepared via the melting method, cobalt nitrate hexahydrate is in the melting state at 80 °C and has a certain fluidity, which can penetrate into the micropores and mesoporous channels of Beta zeolites. After calcination, cobalt oxide nanoparticles with good dispersion can be carried out on the inner and outer surface of the pores of Beta zeolites, thus reducing the specific surface area of Beta zeolites and reducing the volume of micropores and mesoporous pores.

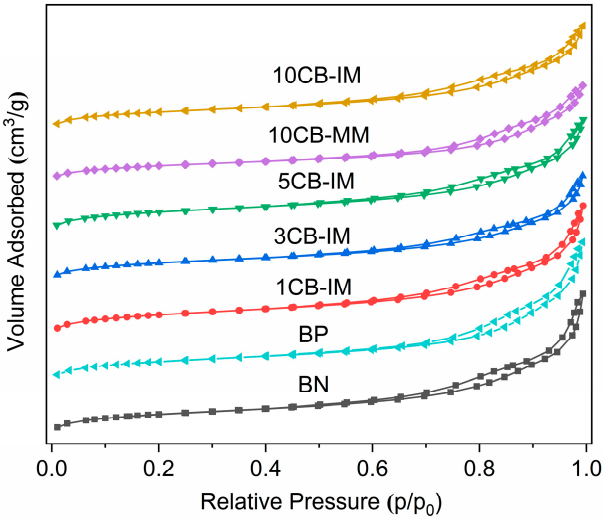


Figure 4. N_2 adsorption–desorption curves of different samples.

Table 1. Texture properties of different samples.

Sample	Surface Area ($m^2 \cdot g^{-1}$)			Volume ($cm^3 \cdot g^{-1}$)		
	BET	Micro.	Exter.	Total	Micro.	Meso.
BP	491	359	132	0.47	0.15	0.32
BN	515	372	143	0.61	0.17	0.44
1CB-IM	458	319	139	0.56	0.15	0.41
3CB-IM	446	316	130	0.50	0.16	0.34
5CB-IM	439	314	125	0.51	0.15	0.36
10CB-MM	416	294	122	0.47	0.13	0.34
10CB-IM	407	286	121	0.44	0.11	0.33

The pore size distributions of BJH models for different catalyst samples are shown in Figure 5. The BN of acid-treated Beta zeolite samples contains mesoporous pores in the range of 5–30 nm, which is due to the dealumination and partial dissolution of Beta zeolite samples with acid treatment, forming the morphology of nanocrystalline-aggregated structure. The process of dealumination and partial dissolution is random, resulting in irregular 5–30 nm mesoporous channels with wide pore size distribution. Using acid-treated Beta zeolite as support, the pore size distribution of xCB-IM series catalysts prepared via the impregnation method is basically the same as that of BN samples, with mesoporous channels in the range of 5–30 nm. At the same time, it can be seen from Figure 5 that, compared with BN samples, the peak height of pore size distribution curve decreases with the increase in cobalt loading. This is due to the fact that with the increase in cobalt loading, more cobalt oxide particles enter into the mesoporous channels of zeolites, blocking part of the mesoporous channels, resulting in a decrease in the number of

mesopores. Compared with the 10CB-IM samples prepared via the impregnation method, the pore size distribution of the 10CB-MM samples prepared via the melting method shifted from 5–30 nm to 6–40 nm.

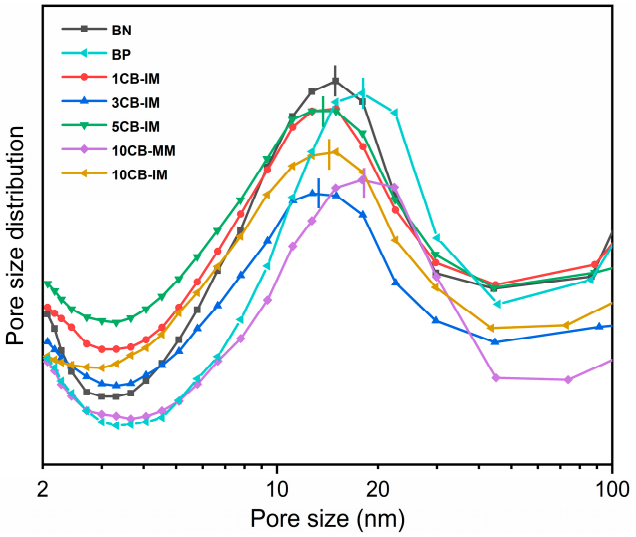


Figure 5. Pore size distribution of different samples.

Ammonia temperature-programmed desorption (NH_3-TPD) is often used to characterize the acid properties of analytical catalysts. As a basic molecule, ammonia can be adsorbed on the acidic sites of the catalyst. The increase in ammonia desorption temperature is accompanied by the increase in the acid strength of the acid center [16]. The ammonia desorption peaks of catalysts can be divided into three types according to the temperature range: weak acid peak (20–200 °C), medium–strong acid peak (200–360 °C) and strong acid peak (360–550 °C) [18–22].

In this work, NH_3-TPD was used to characterize the acid content and acid strength of the Co/Beta catalysts. The NH_3-TPD curve and acid quantity fitting results of different samples are shown in Figure S2 and Table 2, respectively. First, it can be seen from Figure S2 and Table 2 that the acid-treated Beta zeolite BN samples have a high strong acid content and weak acid content. According to the literature report, if the strong acid content of zeolite catalyst is too high, it will improve the catalytic cracking activity, make the hydrocarbon distribution of Fischer–Tropsch products shift to the low-carbon products and improve the selectivity of low-carbon products such as methane and C_2-C_7, which is not conducive to enhancing C_8-C_{16} hydrocarbon selectivity [23]. The SiO_2/Al_2O_3 of the original Beta zeolite is 25, which contains large numbers of strong acid sites. In order to reduce the strong acid content of the Beta zeolite, we pretreated the Beta zeolite with a high concentration of nitric acid. The acid treatment can greatly remove framework aluminum of the Beta zeolite and reduce the strong acid content of the zeolite. At the same time, strong acid treatment can also partially dissolve Beta zeolite particles, form nanocrystalline-aggregated structure and improve the mesoporous content and diffusivity of the catalyst. Thus, Co-Beta catalysts with suitable acid properties and hierarchical pore properties are obtained.

For the xCB-IM series catalysts prepared via the impregnation method, with the increase in cobalt loading, the amount of strong acid decreased gradually, while the amount of medium acid increased gradually. The reduction in strong acidity and increase in medium acidity is ascribed to the interaction between Co^{2+} ions and strong acid sites (Si–OH–Al), which could generate new medium acid sites. Moreover, the interaction between large CoO_x nanoparticles and strong acid sites can also reduce the strong acid amount and increase the medium strong acid amount. The 10CB-MM sample prepared via the melting method also shows a reduction in strong acid sites and an increase in medium acid sites, which is caused by the interaction between small CoO_x nanoparticles and strong acid sites during the melting and calcination process. Because the acid property of the catalyst has

an important influence on the catalytic performance of syngas-to-aviation kerosene, the acid strength and acid content of the catalyst are adjusted by acid treatment and metal cobalt oxide loading. The product distribution of the reaction from syngas (CO and H_2) to aviation kerosene can be indirectly controlled. The structure–activity relationship between the acid properties and catalytic performance of catalysts will be further studied in the form of catalytic tests.

Table 2. Fitting results of acid content of different samples.

Sample	Acid Amount (mmol/g)			
	Weak	Medium	Strong	Total
BN	0.78	-	0.67	1.45
1CB-IM	0.89	0.49	0.52	1.9
3CB-IM	0.83	0.55	0.43	1.81
5CB-IM	0.76	0.62	0.39	1.77
10CB-MM	0.62	0.68	0.31	1.61
10CB-IM	0.65	0.76	0.23	1.64

Figure 6 shows the UV-Vis spectra of different samples. For Beta zeolite BN samples, the absorption curve is almost a horizontal straight line, and there is no characteristic absorption band. For the sample xCB-IM, prepared via the impregnation method, the absorption band fluctuates in the range of 400–800 nm. The characteristic band produced when the absorption band is in the range of 400–550 nm and 600–750 nm is assigned to the ligand-metal charge transfer of $O^{2-} \rightarrow Co^{2+}$ and $O^{2-} \rightarrow Co^{3+}$ in Co_3O_4 [24]. The above results showed that the samples prepared via the impregnation method all contained Co^{2+} and Co^{3+}. It was observed that the absorption band heights of 440 nm, 505 nm, 650 nm, 700 nm and 745 nm increased with the increase in cobalt loading, indicating that the content of Co_3O_4 on the catalyst also increased [25]. The UV spectra of the 10CB-MM samples prepared via the melting method are similar to those of the 10CB-IM samples prepared via the impregnation method, indicating that 10CB-MM samples prepared via the melting method also contain Co_3O_4 species.

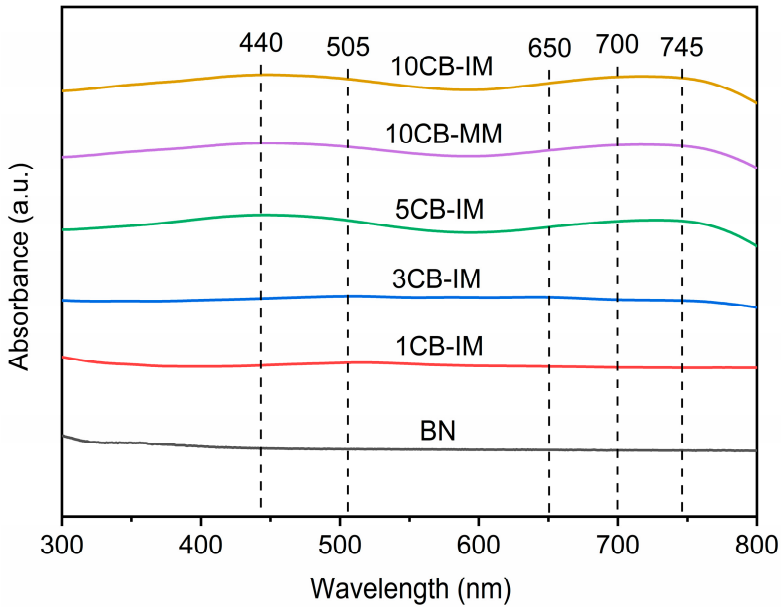


Figure 6. UV-Vis spectra of different samples.

The reducibility of cobalt species in Co/Beta series catalysts can be analyzed by H_2-TPR characterization of 1CB-IM, 10CB-IM and 10CB-MM, as shown in Figure 7. Generally, there are two reduction peaks at different positions in the three catalyst samples, and the

two reduction peaks belong to the reduction peaks of Co^{3+} ion to Co^{2+} ion and Co^{2+} ion to Co^0, indicating the valence change process of cobalt species from Co_3O_4 to CoO and then to elemental Co [25,26].

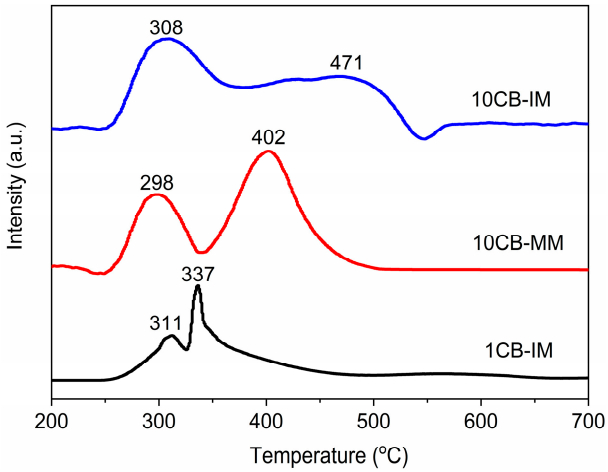


Figure 7. H_2-TPR curves of different samples.

In addition, the position of the H_2-TPR reduction peak reflects the reducibility of the catalyst. Compared with the 10CB-IM samples prepared via the impregnation method, the positions of the two reduction peaks of the 10CB-MM samples prepared via the melting method move forward as a whole, which indicates that the Co_3O_4 species of the samples prepared via the melting method are more easily reduced under the same cobalt loading, which is attributed to the interaction between the Co_3O_4 species and the support of the catalyst prepared via the melting method being weak, so it is more easily reduced. However, some cobalt ion species of the catalysts prepared by impregnation have a strong interaction with the Si–OH–Al acid sites of zeolites, and the particle size of Co_3O_4 species is larger, which makes it more difficult to reduce the cobalt species. By comparing the samples with different loading via the impregnation method, it is found that the first peak temperature of the reduction peak of the 10CB-IM samples is lower than that of the 1CB-IM samples, while the second peak temperature of the reduction peak of 10CB-IM samples is higher than that of the 1CB-IM samples. The results show that the 10CB-IM samples contain both easy-to-reduce Co_3O_4 species and difficult-to-reduce Co_3O_4 species, which is due to the uneven particle size of Co_3O_4 species in the high-loading 10CB-IM catalyst samples prepared via the impregnation method.

The catalytic performance of different samples for syngas-to-aviation kerosene is shown in Table 3. Firstly, 0.5g catalyst is reduced for 8 h at 400 °C in hydrogen stream. After the catalyst is reduced, the raw material of syngas with H_2/CO volume ratio of 2 is injected at the gas flow rate of 26 mL/min and reacted for 24 h at the temperature of 230 °C; the GHSV is 3120 mL/(g_{cat}·h), and the pressure is 3 MPa. The product analysis results of the catalyst reaction for 24 h are listed in Table 3. And, the CO conversions with time on stream of different samples are shown in Figure 8.

During the whole reaction period, the conversion of 1CB-IM sample remains at a low level (Figure 8). After 24 h of reaction, the conversion of CO hydrogenation is only 2.2%, and the CH_4 selectivity is the highest, while the selectivity of C_8-C_{16} aviation kerosene component is the lowest. This is because cobalt is the active center for initiating a CO hydrogenation reaction and chain growth reaction [27], the cobalt loading of 1CB-IM sample is too low (1 wt%), the number of active sites for CO hydrogenation reaction and chain growth reaction is insufficient, resulting in a low CO conversion.

As seen in Figure 8, comparing the 10CB-MM sample prepared via the melting method and the 10CB-IM sample prepared via the impregnation method, we can find the CO conversion of the 10CB-MM sample is higher than that of the 10CB-IM sample during the whole reaction period. Meanwhile, the declining rate of conversion of the 10CB-MM

sample is slower than that of the 10CB-IM sample, indicating that the 10CB-MM sample has a higher CO hydrogenation catalytic activity and stability than the 10CB-IM sample.

Table 3. Catalytic performance of different samples for syngas-to-aviation kerosene.

Sample	CO Conversion (%)	Selectivity (%)					
		CH_4	C_2-C_7	C_8-C_{16}	C_{17+}	CO_2	O/P [a]
1CB-IM	2.2	26.8	38.9	19.3	7.2	7.7	0.24
3CB-IM	8.4	23.0	38.0	24.5	7.5	7.0	0.21
5CB-IM	14.3	21.1	35.3	28.1	9.7	5.7	0.17
10CB-MM	34.6	14.0	31.2	40.2	10.4	4.2	0.12
10CB-IM	29.7	15.8	32.4	36.2	10.6	4.9	0.14

[a] O/P: (C_8-C_{16}n(olefin)/C_8-C_{16}n(paraffin)).

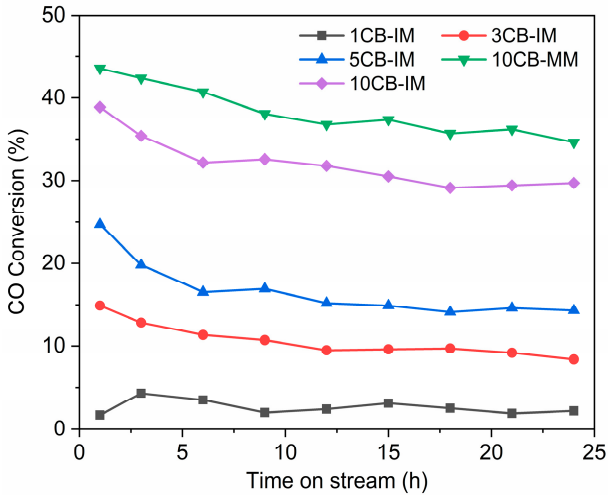


Figure 8. CO conversion of different samples.

For the xCB-IM series catalysts prepared via the impregnation method, the CO conversion and the selectivity of the C_8-C_{16} component both increase with the increase in cobalt loading, and the mole ratio of olefin and paraffin (O/P) in the C_8-C_{16} products gradually decrease with the increase in cobalt loading (Table 3). The increase in CO conversion and the decrease in O/P are due to the fact that cobalt is the active center for catalytic initiation of CO hydrogenation reaction and chain growth reaction [27]. With the increase in cobalt loading, the number of active centers for CO conversion and hydrogenation reaction is increasing [28–30]. On the one hand, it can continuously increase the CO conversion. On the other hand, it can also promote the hydrogenation of olefins, improve the alkane selectivity, reduce the olefin selectivity and lead to the decrease in the O/P ratio.

In addition, the increasing selectivity of the C_8-C_{16} component is due to the increasing trend of cobalt species particle size with the increase in cobalt loading. The larger the cobalt species size, the weaker the interaction between the cobalt species and Beta zeolite support, and the more easily it is reduced, which is beneficial for the improvement in the selectivity of high-carbon-number hydrocarbons [31]. Moreover, with the increase in cobalt loading, the amount of strong acid in the catalyst decreases gradually, and the amount of medium acid increases gradually, and the decrease in strong acid content is beneficial to inhibit the catalytic cracking of Fischer–Tropsch synthesis products. Thus, it is beneficial for the distribution of Fischer–Tropsch synthesis products to move to high-carbon-number hydrocarbon products [23].

Compared with the 10CB-IM samples prepared via the impregnation method, the 10CB-MM catalyst samples prepared via the melting method have higher CO conversion and C_8-C_{16} aviation kerosene component selectivity and a lower O/P ratio. After 24 h of reaction, the CO conversion of the 10CB-MM catalyst prepared via the melting method

reaches 34.6%. The selectivity of the C_8-C_{16} aviation kerosene component is 40.2%. This is due to the fact that the 10CB-MM sample prepared via the melting method is equivalent to the 10CB-IM sample prepared via the impregnation method. The CoO_x species prepared via the melting method has a smaller particle size, higher dispersion, easier reduction, higher CO hydrogenation and chain growth catalytic activity, more suitable acid strength and acid content, and can cut long-chain hydrocarbon molecules into short-chain hydrocarbon molecule products in the C_8-C_{16} range through an appropriate amount of strong acid sites. As a result, the selectivity of the C_8-C_{16} aviation kerosene component in the catalytic products is higher, and the O/P ratio is lower [23,31].

This process can achieve the goal of direct and highly selective preparation of aviation kerosene hydrocarbon products from syngas (CO and H_2) without subsequent complex processing steps such as hydrocracking and hydrofining, which provides a new idea for the production of aviation kerosene in the Fischer–Tropsch synthesis industry.

4. Conclusions

In this work, a new preparation method of a hierarchical Co/Beta metal-zeolite bifunctional catalyst is proposed by a two-step method. The first step is to prepare hierarchical Beta zeolite support by acid treatment, the second step is to prepare a hierarchical Co/Beta catalyst via the melting method. This hierarchical Co/Beta catalyst prepared via the melting method can directly and highly selectively produce a C_8-C_{16} aviation kerosene component from syngas (CO and H_2). Compared with the 10CB-IM catalyst prepared via the impregnation method, the Co/Beta catalyst sample 10CB-MM, prepared via the melting method, has smaller, more highly dispersed Co_3O_4 nanoparticles and more suitable acid properties, resulting in a higher conversion of CO (34.6%) and a higher selectivity of the C_8-C_{16} (40.2%) aviation kerosene component. This process can achieve the goal of direct and highly selective preparation of aviation kerosene hydrocarbon products from syngas without subsequent complex processing steps such as hydrocracking and hydrofining, which provides a new idea for the production of aviation kerosene in the Fischer–Tropsch synthesis industry.

Supplementary Materials: The following supporting information can be downloaded at: https://www.mdpi.com/article/10.3390/cryst13071053/s1, Figure S1: TEM images of different samples; Figure S2: NH_3-TPD curves of different samples.

Author Contributions: Conceptualization, Y.Z., J.W. and J.Z.; methodology, Y.Z and Z.L.; software, X.L.; validation, W.Z., X.L. and L.M.; formal analysis, W.Z. and X.L.; data curation, W.Z. and X.L.; writing—original draft preparation, Y.Z.; writing—review and editing, Z.L.; visualization, Y.Z. and Z.Z.; supervision, J.W. and Z.L.; project administration, Y.Z. and J.W.; funding acquisition, J.W. and Z.L. All authors have read and agreed to the published version of the manuscript.

Funding: This research was funded by Scientific Research and Technology Development Project of China National Petroleum Corporation (DQZX-KY-21-018) and Guiding Innovation Fund of Northeast Petroleum University (032/15071202203).

Data Availability Statement: Data is unavailable due to privacy restrictions.

Conflicts of Interest: The authors declare no conflict of interest.

References

1. Ng, K.S.; Farooq, D.; Yang, A. Global biorenewable development strategies for sustainable aviation fuel production. *Renew. Sustain. Energy Rev.* **2021**, *150*, 111502. [CrossRef]
2. Li, M.; Zhao, W.; Xu, Y.; Zhao, Y.; Yang, K.; Tao, W.; Xiao, J. Comprehensive Life Cycle Evaluation of Jet Fuel from Biomass Gasification and Fischer–Tropsch Synthesis Based on Environmental and Economic Performances. *Ind. Eng. Chem. Res.* **2019**, *58*, 19179–19188. [CrossRef]
3. Timko, M.T.; Herndon, S.C.; De La Rosa Blanco, E.; Wood, E.C.; Yu, Z.; Miake-Lye, R.C.; Knighton, W.B.; Shafer, L.; DeWitt, M.J.; Corporan, E. Combustion products of petroleum jet fuel, a Fischer–Tropsch synthetic fuel, and a biomass fatty acid methyl ester fuel for a gas turbine engine. *Combust. Sci. Technol.* **2011**, *183*, 1039–1068. [CrossRef]

4. Jürgens, S.; Oßwald, P.; Selinsek, M.; Piermartini, P.; Schwab, J.; Pfeifer, P.; Bauder, U.; Ruoff, S.; Rauch, B.; Köhler, M. Assessment of combustion properties of non-hydroprocessed Fischer-Tropsch fuels for aviation. *Fuel Process. Technol.* **2019**, *193*, 232–243. [CrossRef]
5. De Klerk, A. Aviation turbine fuels through the Fischer–Tropsch process. In *Biofuels for Aviation*; Elsevier: Amsterdam, The Netherlands, 2016; pp. 241–259.
6. Cai, Y.; Xu, X.; Wang, H.; Wang, L.; Chen, L.; Li, R.; Ding, J.; Wan, H.; Guan, G. Bifunctional Co/Al-SBA-15 catalyst with tunable acidity for selective production of aviation fuel. *Ind. Eng. Chem. Res.* **2018**, *57*, 3844–3854. [CrossRef]
7. Boymans, E.; Nijbacker, T.; Slort, D.; Grootjes, S.; Vreugdenhil, B. Jet Fuel Synthesis from Syngas Using Bifunctional Cobalt-Based Catalysts. *Catalysts* **2022**, *12*, 288. [CrossRef]
8. Sineva, L.; Asalieva, E.Y.; Mordkovich, V. The role of zeolite in the Fischer–Tropsch synthesis over cobalt–zeolite catalysts. *Russ. Chem. Rev.* **2015**, *84*, 1176. [CrossRef]
9. Lu, Y.; Lee, T. Influence of the feed gas composition on the Fischer-Tropsch synthesis in commercial operations. *J. Nat. Gas Chem.* **2007**, *16*, 329–341. [CrossRef]
10. Sauciuc, A.; Abosteif, Z.; Weber, G.; Potetz, A.; Rauch, R.; Hofbauer, H.; Schaub, G.; Dumitrescu, L. Influence of operating conditions on the performance of biomass-based Fischer–Tropsch synthesis. *Biomass Convers. Biorefinery* **2012**, *2*, 253–263. [CrossRef]
11. Nakanishi, M.; Uddin, M.A.; Kato, Y.; Nishina, Y.; Hapipi, A.M. Effects of preparation method on the properties of cobalt supported β-zeolite catalysts for Fischer-Tropsch synthesis. *Catal. Today* **2017**, *291*, 124–132. [CrossRef]
12. Renzini, M.S.; Lerici, L.C.; Sedran, U.; Pierella, L.B. Stability of ZSM-11 and BETA zeolites during the catalytic cracking of low-density polyethylene. *J. Anal. Appl. Pyrolysis* **2011**, *92*, 450–455. [CrossRef]
13. Wang, B.; Yan, X.; Zhang, X.; Zhang, H.; Li, F. Citric acid-modified beta zeolite for polyoxymethylene dimethyl ethers synthesis: The textural and acidic properties regulation. *Appl. Catal. B Environ.* **2020**, *266*, 118645. [CrossRef]
14. Hao, Q.-Q.; Zhao, Y.-H.; Yang, H.-H.; Liu, Z.-T.; Liu, Z.-W. Alumina grafted to SBA-15 in supercritical CO_2 as a support of cobalt for Fischer–Tropsch synthesis. *Energy Fuels* **2012**, *26*, 6567–6575. [CrossRef]
15. Zhang, K.; Fernandez, S.; Lawrence, J.A., III; Ostraat, M.L. Organotemplate-free β zeolites: From zeolite synthesis to hierarchical structure creation. *ACS Omega* **2018**, *3*, 18935–18942. [CrossRef]
16. Chen, C.; Zhang, S.; Wang, Z.; Yuan, Z.-Y. Ultrasmall Co confined in the silanols of dealuminated beta zeolite: A highly active and selective catalyst for direct dehydrogenation of propane to propylene. *J. Catal.* **2020**, *383*, 77–87. [CrossRef]
17. Qiao, Y.; Yang, M.; Gao, B.; Wang, L.; Tian, P.; Xu, S.; Liu, Z. Creation of hollow SAPO-34 single crystals via alkaline or acid etching. *Chem. Commun.* **2016**, *52*, 5718–5721. [CrossRef]
18. Li, C.J.; Zhang, Y.J.; Chen, H.; He, P.Y. Highly-effective production of renewable energy dimethyl ether over geopolymer-based ferrierite. *Fuel* **2021**, *293*, 120486. [CrossRef]
19. Babu, G.P.; Hegde, S.G.; Kulkarni, S.B.; Ratnasamy, P. Active centres over HZSM5 zeolites: I. Xylene isomerization. *J. Catal.* **1983**, *81*, 471–477. [CrossRef]
20. Yu, Y.; Xi, Z.; Zhou, B.; Jiang, B.; Liao, Z.; Yang, Y.; Wang, J.; Huang, Z.; Sun, J.; Yang, Y. Acidity Modification of ZSM-5 for Methane Conversion in Co-feeding Method with MTA Reaction. *Chem. Res. Chin. Univ.* **2022**, *38*, 1012–1017. [CrossRef]
21. Zhai, Y.; Shang, Y.; Zhang, L.; Meng, X.; Gong, Y.; Zheng, L.; Zhang, J.; Liu, P. Hydrothermally modified nanosheet ZSM-5 with MnOx nanoparticles and its high MTP performance. *Microporous Mesoporous Mater.* **2021**, *326*, 111374. [CrossRef]
22. Zhang, Z.; Wang, P.; Wu, Z.; Yue, C.; Wei, X.; Zheng, J.; Xiang, M.; Liu, B. Efficient synthesis of niobium pentoxide nanowires and application in ethanolysis of furfuryl alcohol. *RSC Adv.* **2020**, *10*, 5690–5696. [CrossRef] [PubMed]
23. Javed, M.; Cheng, S.; Zhang, G.; Amoo, C.C.; Wang, J.; Lu, P.; Lu, C.; Xing, C.; Sun, J.; Tsubaki, N. A facile solvent-free synthesis strategy for Co-imbedded zeolite-based Fischer-Tropsch catalysts for direct gasoline production. *Chin. J. Catal.* **2020**, *41*, 604–612. [CrossRef]
24. Kojima, K.; Taguchi, H.; Matsuda, J. Optical and magnetic properties of cobalt (2+) ions in dried and heated silica gels prepared by the sol-gel process. *J. Phys. Chem.* **1991**, *95*, 7595–7598. [CrossRef]
25. Selvam, P.; Mohapatra, S. Synthesis and characterization of divalent cobalt-substituted mesoporous aluminophosphate molecular sieves and their application as novel heterogeneous catalysts for the oxidation of cycloalkanes. *J. Catal.* **2005**, *233*, 276–287. [CrossRef]
26. Verberckmoes, A.A.; Weckhuysen, B.M.; Schoonheydt, R.A. Spectroscopy and coordination chemistry of cobalt in molecular sieves. *Microporous Mesoporous Mater.* **1998**, *22*, 165–178. [CrossRef]
27. Ernst, B.; Hilaire, L.; Kiennemann, A. Effects of highly dispersed ceria addition on reducibility, activity and hydrocarbon chain growth of a Co/SiO2 Fischer–Tropsch catalyst. *Catal. Today* **1999**, *50*, 413–427. [CrossRef]
28. Sun, S. The Reaction Performances and Characterization of Fischer-Tropsch Synthesis Co/SiO_2 Catalysts Prepared from Mixed Cobalt Salts. *Appl. Catal. A* **2000**, *202*, 121–131. [CrossRef]
29. Jacobs, G.; Das, T.K.; Zhang, Y.; Jinlin, L.; Racoillet, G.; Davis, B.H. Fischer-tropsch synthesis: Support, loading and promoter effects on the reducibility of cobalt catalysts. *Appl. Catal. A. Gen.* **2002**, *233*, 263–281. [CrossRef]

30. Tavasoli, A.; Abbaslou, R.; Trepanier, M.; Dalai, A.K. Fischer-Tropsch Synthesis Over Cobalt Supported on Carbon Nanotubes in a Slurry Reactor. *Appl. Catal. A Gen.* **2008**, *345*, 134–142. [CrossRef]
31. Trépanier, M.; Tavasoli, A.; Dalai, A.K.; Abatzoglou, N. Co, Ru and K loadings effects on the activity and selectivity of carbon nanotubes supported cobalt catalyst in Fischer–Tropsch synthesis. *Appl. Catal. A Gen.* **2009**, *353*, 193–202. [CrossRef]

Disclaimer/Publisher's Note: The statements, opinions and data contained in all publications are solely those of the individual author(s) and contributor(s) and not of MDPI and/or the editor(s). MDPI and/or the editor(s) disclaim responsibility for any injury to people or property resulting from any ideas, methods, instructions or products referred to in the content.